Influence of the Relative Amounts of Crystalline and Amorphous Phases on the Mechanical Properties of Polyamide-6 Nanocomposites

João Gargalaka, Jr., Ricardo A. A. Couto, Vera R. L. Constantino, Henrique E. Toma, Koiti Araki

Departamento de Química Fundamental, Instituto de Química, Universidade de São Paulo, Cidade Universitária, CEP 05508-000, São Paulo, SP, Brazil

Received 12 September 2011; accepted 18 November 2011
DOI 10.1002/app.36509
Published online 1 February 2012 in Wiley Online Library (wileyonlinelibrary.com).

ABSTRACT: The relative amounts of amorphous and crystalline γ- and α-phases in polyamide-6 nanocomposites, estimated from the deconvolution of X-ray diffraction peaks using Gaussian functions, correlates with their mechanical, thermomechanical, and barrier properties. The incorporation of organoclay platelets (Cloisite 15A and 30B) induced the crystallization of the polymer in the γ form at expense of the amorphous phase, such that 1–2 wt % of Cloisite is enough to enhance the mechanical and the thermomechanical properties. However, higher nanofiller loads were necessary to achieve good barrier effects, because this property is mainly dependent on the tortuous path permeation mechanism of the gas molecules through the nanocomposite films. © 2012 Wiley Periodicals, Inc. J Appl Polym Sci 125: 3239–3249, 2012

Key words: polyamide; Cloisite; nanocomposites; mechanical properties; barrier effect

INTRODUCTION

Nanocomposites can be prepared by homogeneous dispersion of zero, one, and two-dimensional nanomaterials, such as nanospheres, nanotubes, and nanoplatelets, in organic polymeric matrices. They are interesting materials since can exhibit notable improvements in physicochemical and/or mechanical properties[1–7] as compared to the pristine polymer or conventional composites.

The first developments of such organic–inorganic hybrid materials were carried out by Toyota that started the production of automotive parts using polyamide-6 (PA-6)/clay nanocomposites.[8] In fact, the incorporation of small amounts of layered aluminosilicates such as montmorillonite (MMT) diminished the polymer flammability,[9–12] enhanced its thermomechanical properties, and reduced significantly the weight, thus improving the performance and efficiency of vehicles. However, such materials only became more readily available after the development of fabrication methods based on the direct incorporation of nanofillers into the melted matrix by Vaia et al.[13]

Among the inorganic nanoparticles available for preparation of organic polymeric nanocomposites, natural and synthetic clays (layered silicates) have deserved great attention of researchers at academia and industry.[1] Among the most commonly used matrices for polymer–clay nanocomposites (PCN) are PA-6,[1] poly(vinyl chloride),[14] polyurethane,[15] styrene butadiene rubber,[16] Nafion,[17] poly(aniline),[18] poly(lactic acid),[19] polymeric hydrogels,[20] and bacterial cellulose.[21]

The characteristics of PCN materials are strongly dependent on the extent of clay exfoliation, which is defined by processing parameters such as temperature, pressure, type of extruder, and design of screw, as well as by the functionalization of the nanofiller and the strength of the interaction between the dispersed nanomaterial and the polymeric matrix.[5,21] Generally, the viscosity, temperature, and extruder rotation speed should be carefully controlled to have high enough shear energy to promote exfoliation/intercalation processes.[22]

To get a tough interfacial interaction between the polymeric matrix and the nanofiller surface, hydrophobic organic polymers should be mixed with clays having organic surfactants in between the layers and at the external surfaces, known as organoclays. Cloisites are commercially available natural MMT clays whose cations were exchanged by quaternary ammonium cations with long hydrocarbon chains and low polarity, making the two dissimilar phases

Additional Supporting Information may be found in the online version of this article.

Correspondence to: K. Araki (koiaraki@iq.usp.br).

Contract grant sponsor: Brazilian Agencies Fundação de Amparo à Pesquisa do Estado de São Paulo (FAPESP) and Conselho Nacional de Desenvolvimento Científico e Tecnológico (CNPq).

compatible and ensuring the formation of interesting nanocomposite materials.

Fornes and Paul[23] prepared PA-6/MMT nanocomposites using low, medium, and high molecular weight resins. The X-ray diffraction (XRD) and transmission electron microscopy (TEM) data revealed that the fraction of exfoliated/intercalated clay increased as a function of the polymer molecular weight, reflecting the influence of the melt viscosity, and consequently of the shear energy, on the characteristics of the resultant materials. In fact, PA-6/MMT composites prepared with low molecular weight resins showed some degree of intercalation and exfoliation, whereas those prepared with medium to high molecular weight resins exhibited almost completely exfoliated clay particles.

Liu et al.[24] prepared PA-6 nanocomposites in a twin-screw extruder using 1–18 wt % of a MMT modified with octadecylammonium cation. Polymer intercalation took place when the clay loads were greater than 10 wt % as indicated by the expansion of the interlayer distances (15.5–36.8 Å). However, for lower amounts of clay, the 001 diffraction peak was not well defined enough to allow a precise measurement. In addition, the XRD and differential scanning calorimetry (DSC) data indicated that the nanocomposites have a higher degree of crystallinity than the pristine PA-6, and that the clay incorporation promoted the formation of the γ-phase in detriment of the α-phase.

Russo et al.[25] studied the influence of the processing parameters in a three-stage twin-screw extruder, followed by reprocessing in a single-screw extruder, on the properties of PA-6/Cloisite 30B nanocomposites. The XRD and TEM results indicated that the reprocessing changed the clay morphology and the fraction of exfoliation, thus degrading the mechanical properties. This was attributed to decomposition of the quaternary ammonium cation and consequent reconstruction of tactoids.

Despite the extensive works that have been carried out with PA-6/MMT nanocomposites, only few of them were focused on the influence of the amount of organoclay in the crystallization process.[23,26–32] Fornes and Paul[23] carried out a seminal work on that phenomena, but the correlation with other physicochemical properties has not been systematically explored yet. Accordingly, in this work, the study of the influence of Cloisite (15A and 30B) nanofiller on the polymorphism, as well as the influence of the degree of crystallinity on the mechanical, thermomechanical, and gas diffusion properties of PA-6 nanocomposites are described.

EXPERIMENTAL

All samples were prepared with Akulon F-136E, a nucleated high viscosity PA-6 resin, from DSM Engineering Plastics. The organophillized clay additives Cloisite 15A and 30B, from Southern Clay Products, prepared with natural MMT and quaternary ammonium salts, were used to prepare the PA-6/clay polymeric nanocomposites. Cloisite 15A is functionalized with 125 mequiv/100 g of $[N(CH_3)_2(HT)_2]^+Cl^-$, where HT is a long saturated alkyl chain with ~ 65% C18, ~ 30% C16, and ~ 5% C14. Cloisite 30B is functionalized with 90 mequiv/100 g of $[N(CH_2CH_2OH)_2(CH_3)(T)]^+Cl^-$ where T is a long saturated alkyl chain with ~ 65% C18, ~ 30% C16, and ~ 5% C14.

Preparation of the nanocomposites

The nanocomposites were prepared in two steps: the PA-6 resin was first processed with 1–10 wt % of Cloisite in a twin-screw extruder and then the pellets were converted into tubular films using a single-screw equipment connected to an accessory for processing by the balloon method. A Werner & Pfleiderer Megacompounder corotational 32-mm double screw extruder, $L/D = 40$, with 11 heating zones and a lateral feeder in the fifth zone, was used in the melting exfoliation/intercalation process. The following temperatures were used in the zones: 1: 230°C, 2–4: 250°C, 5–7: 240°C, and 8–11: 230°C. The average pressure was 200 bar and the rotation speed 900 rpm. A lateral automatic feeder with a small screw coupled to the extruder was used to ensure a homogeneous concentration of clay along the samples. The nanocomposites were extruded through six holes, immediately cooled in a water bath at 20°C and cut in pellets, which were reprocessed into films (150 mm wide and 50 μm thick) using a single-screw extruder with five heating zones (230, 240, 245, 250, and 255°C) and rotation rate of 35 rpm. Eight polymeric nanocomposite samples (10 kg each) were prepared and used in all experiments, by incorporation of 1, 2, 5, and 10 wt % of Cloisite 15A or Cloisite 30B.

Characterization

XRD patterns were registered in a Rigaku Miniflex diffractometer equipped with a Ni filter and operating at 30 kV and 15 mA, in the (2θ) 2–80° range, at scan rate of 0.02° s^{-1}, using Cu-K_α radiation (λ = 1.5451 Å). The polymeric film samples were supported in a perforated aluminum base, used as sample holder. Infrared spectra of PA-6/Cloisite composite samples were collected in a Shimadzu 8800 spectrophotometer coupled with AIM-8600 microscope.

The film thickness was measured at every 5 mm in the transversal direction (TD), with a Mitutoyo Absolute digital micrometer. Tensile strength measurements were performed using an Instron 5564 load cell, using 1-inch wide and 50-mm long

specimens until failure (ASTM D882), at elongation rate of 500 mm min^{-1}, 25°C, and relative humidity of 50%. The tensile strength measurements up to failure, at 100% humidity, were carried out with specimens kept in a water bath (40°C) for 30 min. The puncture resistance (ASTM F1306-90) was measured using pieces of nanocomposite films, fixed in between two metal plates with a circular hole in the middle ($A = 962$ mm^2), by exerting pressure up to rupture with a metal tip moving at 100 mm min^{-1}, according to ASTM standards. The thermomechanical analyses (TMA) were carried out in a TA Instruments, model 2940, TM analyzer, using 5-mm wide and 12-mm long specimens. The elongation was monitored at constant force of 1 N as a function of temperature, which was increased at a rate of 10°C min^{-1} from $T_i = 70$°C.

The permeability of the nanocomposite films to oxygen gas was evaluated at 0 and 95% relative humidity using a Mocon Ox-Tran model 2/22 equipment. The samples ($A = 50$ cm^2) were conditioned in a desiccator containing activated silica-gel for 48 h before carrying out the measurements at 0% humidity, using a constant flux of oxygen and a carrier gas (nitrogen, 10 mL min^{-1}), at 23°C. The measurements at 95% relative humidity were carried out using samples conditioned in a desiccator for 48 h, whose atmosphere was in equilibrium with distilled water at 25°C. All parameters were the same as that used in the dry conditions, except that the carrier and oxygen gas chambers were in equilibrium with distilled water at 1.6 psig, to keep the relative humidity at 95%.

The permeability of the PCN films to water vapor was measured in a Mocon Permatran model 3/33 equipment. The samples ($A = 50$ cm^2) were conditioned for 48 h in a desiccator, whose atmosphere was in equilibrium with distilled water. The experiments were carried out using a vapor-saturated nitrogen gas (100 mL min^{-1}) at 25°C.

RESULTS AND DISCUSSION

In this work, the melt intercalation method was used to prepare PCN materials due to its environmental and processing advantages. In fact, it is compatible with currently used industrial processing methods such as molding by extrusion and injection (at least in the case of PA-6 and other thermoplastics). The incorporation of the clay nanofiller in the PA-6 melt was carried out in a twin-screw extruder, using suitable parameters to get pellets with 1, 2, 5, and 10 wt % of Cloisite 15A and Cloisite 30B, which were reprocessed as films in a single-screw extruder. All samples were homogeneous and transparent but a beige color (characteristic of Cloisite) became more pronounced as the concentration of the organoclay increased. However, no significant development of color due to thermal decomposition of the quaternary ammonium or the formation of heterogeneous phases was observed.

The infrared spectra of pristine PA-6 as well as of the PCN films with 1, 2, 5, and 10 wt % of Cloisite 15A are shown in Figure 1(A). The pristine resin exhibited characteristic symmetric and asymmetric C—H stretching bands at 2850 and 2930 cm^{-1},[33] whereas those at 3310 and 3080 cm^{-1} were assigned to N—H stretching and secondary harmonic modes of amide groups. The strong bands at 1545 and 1640 cm^{-1} can be assigned to C=N/C=C and C=O/C=N stretching vibrational modes.

The spectral profile remained almost unchanged after incorporation of Cloisite 15A or Cloisite 30B in the resin, except for the rise of Si—O stretching and angular deformation bands at 1036, 523, and 461 cm^{-1}, respectively. The intensity of these bands were measured and correlated with the concentration of organoclay in the nanocomposites.[34] The band at 1036 cm^{-1} is particularly interesting because of its high intensity and the absence of other peaks nearby, allowing more precise evaluation of its intensity.

A similar behavior was observed for both PCN series, as shown in Figure 1(B,C). Notice that the intensity of the 1036, 523, and 461 cm^{-1} bands is an exponential function, instead of a linear function, of the wt % of Cloisite. This may be reflecting the degree of exfoliation/dispersion of MMT as the concentration of clay in the nanocomposites was increased. PA-6 is a polymorphic material that can be found in amorphous, γ, and α crystalline phases. The bands at 976 (CONH), 1122 (C—C), and 1234 cm^{-1} (CH_2 and tertiary amide) are generally assigned to the presence of the γ-phase, while the bands at 929, 959 (CONH), and 1201 cm^{-1} are assigned to the α-phase.[35] However, no clear correlation could be found between the intensity of those bands and the fraction of those crystalline phases.

Crystallinity of PA-6 and its nanocomposites

X-Ray diffractometry generally is the technique of choice to study the degree of crystallinity of any material, particularly organic polymeric materials. PA-6 can be found in the monoclinic α-phase and the hexagonal/pseudohexagonal γ-phase.[23] The polymer chains lay parallel and interact with each other by means of hydrogen bonds, but they can be oriented in the same (γ-phase) or in the opposite (α-phase) direction to each other. As a consequence, the angle between the hydrogen bonds and the polymer chains are 60° and 90°, respectively, in those crystalline phases.[26]

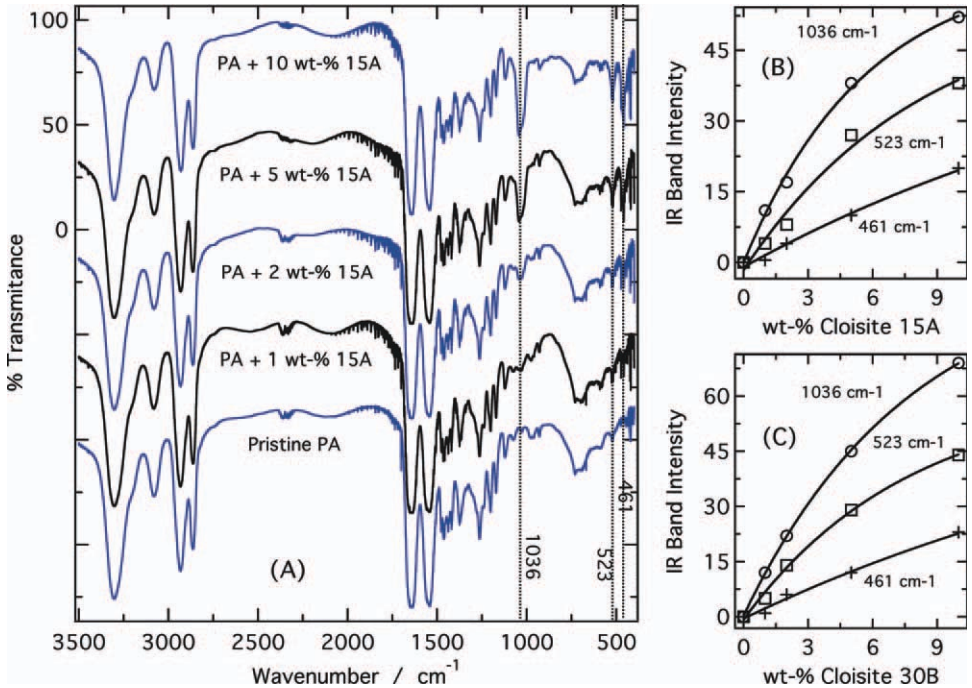

Figure 1 Infrared spectra of pristine PA-6 and the respective nanocomposites with 1, 2, 5, and 10 wt % of Cloisite 15A (A). Plots of the 1036, 523, and 461 cm^{-1} band intensities as a function of Cloisite 15A (B) and Cloisite 30B (C) content. [Color figure can be viewed in the online issue, which is available at wileyonlinelibrary.com.]

According to Fornes and Paul,[23] the XRD pattern of pristine PA-6 exhibits a broad peak around 2θ equal to 21.43° assigned to the amorphous phase, which is superimposed to much narrow peaks at 20.0° and 23.7° assigned to the crystalline α-phase (α_1 and α_2, respectively), and a very sharp peak at 21.3° attributed to the γ-phase. A peak-fitting method was used in this work to show the presence and estimate the contribution of those three phases in the PA-6/Cloisite (15A and 30B) nanocomposite samples.

The XRD pattern of the pristine resin processed in a single-screw extruder showed only a broad peak at 2θ = 21.48° (Fig. 2), that was assigned to an almost completely amorphous material. Only very small contributions from the crystalline phases were found in this case, probably because of the quite fast cooling step used in the processing that precluded the reorganization of the disordered polymer chains present in the melt.[27] No contribution of aluminosilicate peaks could be found even at higher 2θ values, probably because of the low clay concentrations in the nanocomposites (Supporting Information Fig. S1).

Interestingly, the incorporation of 1–10 wt % of Cloisite changed dramatically the crystallinity of the polymer in the respective PCNs, as shown in Figure 2. All of them exhibited a sharp peak at 2θ about 21°, due to the preferential formation of the crystalline γ-phase. In fact, this phase is predominant even at the lowest Cloisite concentration (1 wt %), indicating a very strong polymer chain ordering effect induced by the organoclay nanoflakes. However, it is evident that sharp peak is on the top of a broad halo suggesting the presence of the amorphous phase.[36] A much closer inspection revealed that the base of the sharp peak is broadened by the presence of a low intensity side peak at higher 2θ, that was tentatively assigned to the α_2-peak, while the α_1-peak seems to be hidden under the peak envelope. However, no peaks assignable to Cloisite tactoids could be found because either, their concentration was too low to be detectable by XRD technique, or the organoclay was almost completely exfoliated during the melt processing. The samples with 5 and 10 wt % of Cloisite exhibited XRD peaks in the low 2θ region that could be attributed to tactoids but were broadened and found at higher diffraction angles than that expected for the d_{001} peak of the nanofillers. This result may suggest the presence of tactoids with smaller interlayer distances generated by the thermal decomposition of the respective quaternary ammonium modifiers.[37]

To shed light on the crystallization-inducing properties of Cloisite, a more quantitative analysis was carried out. The contribution of each PA phase was estimated by using a deconvolution method based on asymmetric Gaussian curves implemented in MS-Excel, assuming that the diffraction cross sections are similar. The peak parameters previously found by Fornes and Paul[23] were used as the first approximation, leading to excellent fittings for the pristine

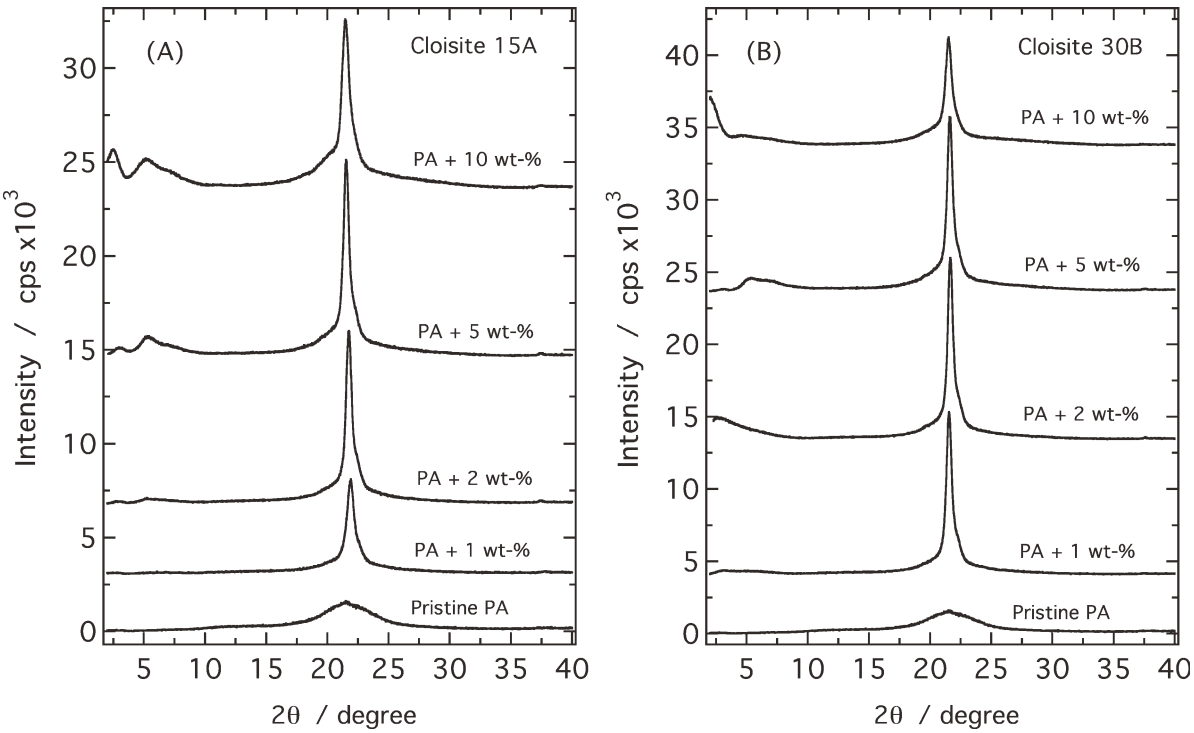

Figure 2 XRD patterns of pristine PA-6 and the nanocomposites with 1, 2, 5, and 10 wt % of (A) Cloisite 15A and (B) Cloisite 30B.

resin and the nanocomposite films (Supporting Information Figs. S2 and S3). Accordingly, a broad Gaussian peak centered at $2\theta = 21.6°$ was used for the amorphous phase, while a sharp peak at 21.5° and two sharp peaks at 20.6° and 22.3° were, respectively, used to account for the γ-phase and α-phase (α_1 and α_2 peaks) contributions. A typical result for the nanocomposite prepared with 1 wt % of Cloisite 15A and Cloisite 30B are shown, respectively, in Figure 3(A,C). Note that there is almost perfect matching between the calculated and experimental curves, indicating that the number of parameters and the XRD peak parameters are suitable for the description of the crystalline and amorphous phases of PA-6/Cloisite nanocomposite materials.

The plots of the integrated area of the peaks corresponding to each phase as a function of the wt % of Cloisite are shown in Figure 3(B,D). The proportion of the γ-phase increased abruptly at the expense of the amorphous phase after incorporation of 1 wt % of Cloisite, while the proportion of the α-phase (α_1- and α_2-peaks) increased only slightly, remaining more or less constant at higher concentrations. In fact, the amount of γ-phase increased from almost 0 to 38–55% after incorporation of 1 wt % of nanofiller. Thus, the organophillized clay platelets should exhibit a very strong capacity to induce crystallization, i.e., to organize the PA hydrocarbon chains around the organic–inorganic interface. However, the contribution of the amorphous phase tended to increase at expense of the γ-phase as the wt % of Cloisite was increased further, as shown in Figure 3(B,C). In addition, the Cloisite 30B was shown to have a much higher crystallization inducing capability than Cloisite 15A. This behavior can be account for only if a certain level of molecular organization is held in the melt by electrostatic and possibly hydrogen bond interactions with the organoclay platelets. The absence of such molecular organization in the melt will imply in a very fast reorganization of the polymer chains induced by the clay during the cooling step, since the pristine PA-6 processed in similar conditions is almost completely amorphous. The last assumption is less probable and can be ruled out because of the mobility constraints imposed by the high viscosity of the melt.

According to computer simulation studies of nylon-6/Cloisite 20A PCNs performed by Scocchi et al.,[38] van der Waals and electrostatic interactions should be considered when analyzing the interaction forces involving PA-6 (a moderate polar polymer), the cationic surfactant and the negatively charged clay platelets. Also, the presence of layered silicates in a polymer matrix can modify the polymer chain conformation next to the clay particle surface inducing pseudoepitaxial nucleation mechanisms.[39] More specifically a tendency of the surfactant and polymer chains to adopt a layered conformation on the clay surface was forwarded by those authors.

In addition, molecular dynamics simulations have suggested that the surfactant molecules (of Cloisite

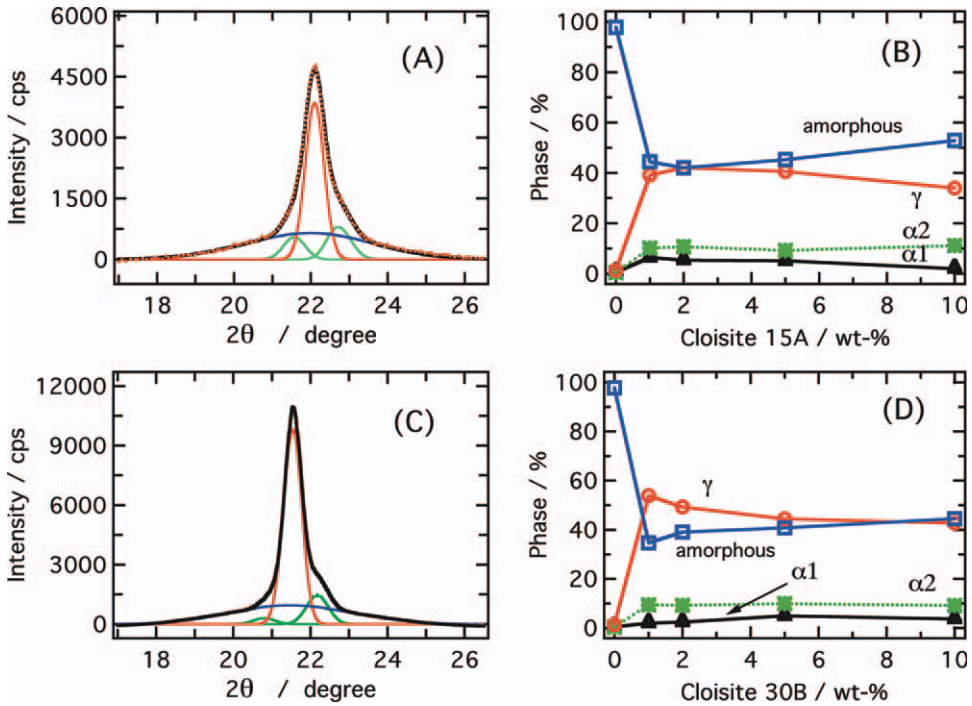

Figure 3 Deconvolution of the diffraction peak at $2\theta \cong 21.6°$ (1 wt % PA-6/Cloisite nanocomposites), based on Gaussian curves, considering the presence of α (green line), γ (red line), and amorphous phases (blue line). Also, the contribution of each crystalline phase (%), estimated by integration of the area under the respective deconvoluted peaks, is plotted as a function of the wt % of (A and B) Cloisite 15A and (C and D) Cloisite 30B. [Color figure can be viewed in the online issue, which is available at wileyonlinelibrary.com.]

20A) are laying flat on the clay surface and the PA-6 chains are resting on them. Only a small fraction of the polymer chains can reach and attach directly to the clay surface, probably through the polar amide groups. Considering that Cloisite 30B has two $-CH_2CH_2OH$ groups in the quaternary ammonium, one can presume that in this case, the interaction between the polymer and the surfactant is stronger than in the Cloisite 15A nanocomposites. Also, the smaller number of long alkyl chains in that quaternary ammonium should generate a less sterically hindered interface, thus allowing a more direct interaction of the polymer chains with the surface of MMT nanoflakes.

In fact, Paul and coworkers[40] showed that well-exfoliated nylon-6/MMT nanocomposites are produced when the surfactant has only one long alkyl chain. However, intercalated and exfoliated clay particles were observed in the nanocomposites when the quaternary ammonium had two alkyl chains. The authors suggested that the surfactant bearing two alkyl chains precludes the approximation of the polyamide to the clay surface by steric effects, hindering the complete exfoliation by melt processing. Thus, the presence of two alkyl groups in the quaternary ammonium cation of Cloisite 15A should make it less suitable for the preparation of PA-6/clay nanocomposites. Probably, both the lower tendency of exfoliation and the lower accessibility of PA-6 chains to the nanoflakes surface are consistent with the lower crystallization induction capability of Cloisite 15A as compared to Cloisite 30B. Those differences will directly influence the thermomechanical properties of the respective nanocomposites, as discussed below.

Thermomechanical properties of the nanocomposite films

The processability of a pristine polymer and its composites can be compared considering the film formation characteristics. Thus, the pellets of pristine PA-6 and the nanocomposites were used to prepare tubular films in a single-screw extruder, keeping the processing parameters constant. The nominal thickness was set to 50 μm, but the average thickness was found to be about 46 μm, except for the 10-wt % PCN samples that showed a contrasting behavior and much higher standard deviations, as shown in Figure 4(A). The expansion of the balloon is strongly influenced by changes in viscosity and flow characteristics during the blow processing. However, the increase in the viscosity of the melt should also change the flow characteristics of the melt inside the extruder, decreasing the actual amount of melt delivered to the ring at the base of the balloon. So,

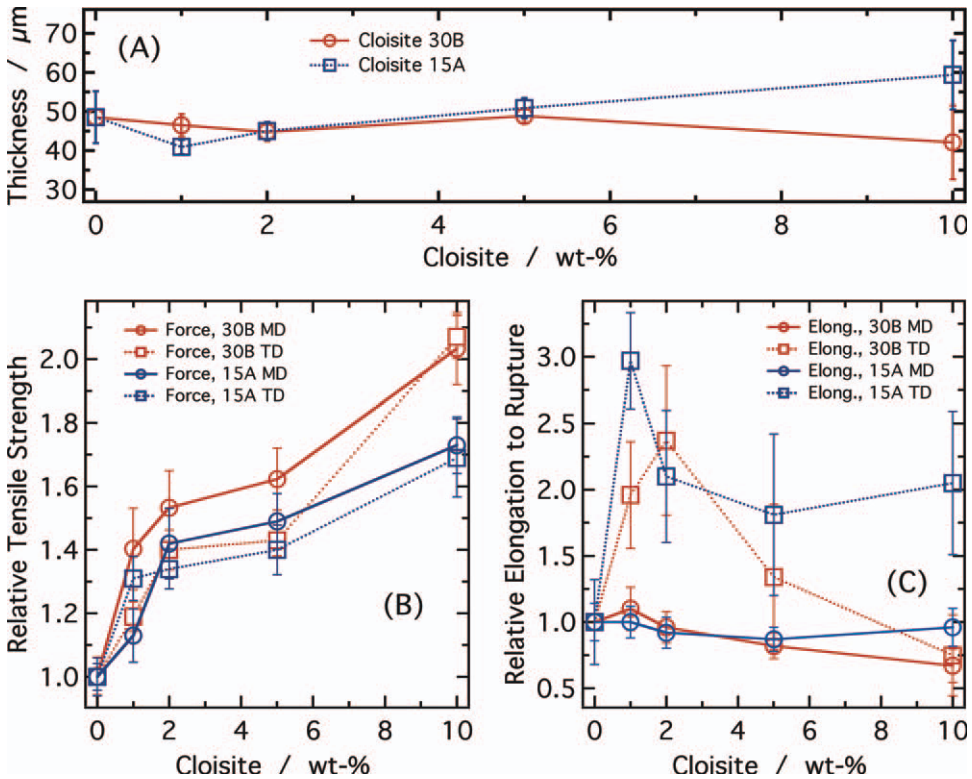

Figure 4 (A) Average thickness of the films prepared with pristine PA and the respective nanocomposites with Cloisite 15A and Cloisite 30B. Each data point is the average of 30 measurements carried out in the transversal direction (TD) to the machine (MD), at room temperature and pressure, and 50% humidity. (B) Relative variation of the tensile strength (value PA: DM = 36.8 and DT = 29.2 MPa) and (C) of elongation until rupture (value PA: DM = 1.85 and DT = 0.69 mm), normalized by the film thickness, for the PCNs with 1, 2, 5, and 10 wt % of Cloisite 30B or Cloisite 15A, at 50% relative humidity. [Color figure can be viewed in the online issue, which is available at wileyonlinelibrary.com.]

the composite prepared with 10 wt % of Cloisite 15A seems to have lower viscosity than the one with the same amount of Cloisite 30B. Interestingly, the variability was also relatively high for the pristine resin suggesting that the incorporation of 1–5 wt % of clay can improve the melt characteristics allowing a better thickness control in the blow processing.

Resistance to traction and elongation

The tensile strength and elongation properties were measured at room temperature and pressure, and 50% humidity, along machine direction (MD) and TD to the MD, to account for the influence of polymer chain preferential orientation. The results are shown as percentage of variation of the traction force and elongation until rupture as compared to the pristine PA-6 films. Larger traction forces (70 and 100%) were registered respectively for the 10-wt % Cloisite 15A and Cloisite 30B composites [Fig. 4(B)], for the films oriented parallel and TD to the MD. A rapid increase in the force was observed for the nanocomposites with 1 and 2 wt % Cloisite than more or less leveling at 5 wt %. This exponential curve paralleled the increase of the proportion of γ-phase in the PCN materials. However, a further increase in the force was observed particularly for the composite with 10 wt % of Cloisite 30B, suggesting the occurrence of new interactions, probably associated with the presence of tactoids and intercalation composites. Summarizing, the tensile strength in the MD was generally larger than in the TD, especially for the Cloisite 30B composites. However, the tensile strength at machine and TD tended to converge at the highest organoclay concentration.

However, the relatively small differences observed in the tensile strength contrasted with the much larger differences observed in the corresponding elongation curves [Fig. 4(C)]. In fact, the elongation in the MD remained almost constant as a function of the Cloisite concentration,[41] except for a slight tendency of decrease observed for the Cloisite 30B nanocomposites, while much larger elongation and variability were found in the TD.[42] The hydrocarbon chains tend to be oriented and stretched along the machine (MD) thus explaining the much higher tendency to flow in the TD. However, the enhanced stiffness of the nanocomposites, particularly at much higher organoclay concentrations, should be accompanied by a decrease in the elongation, as observed

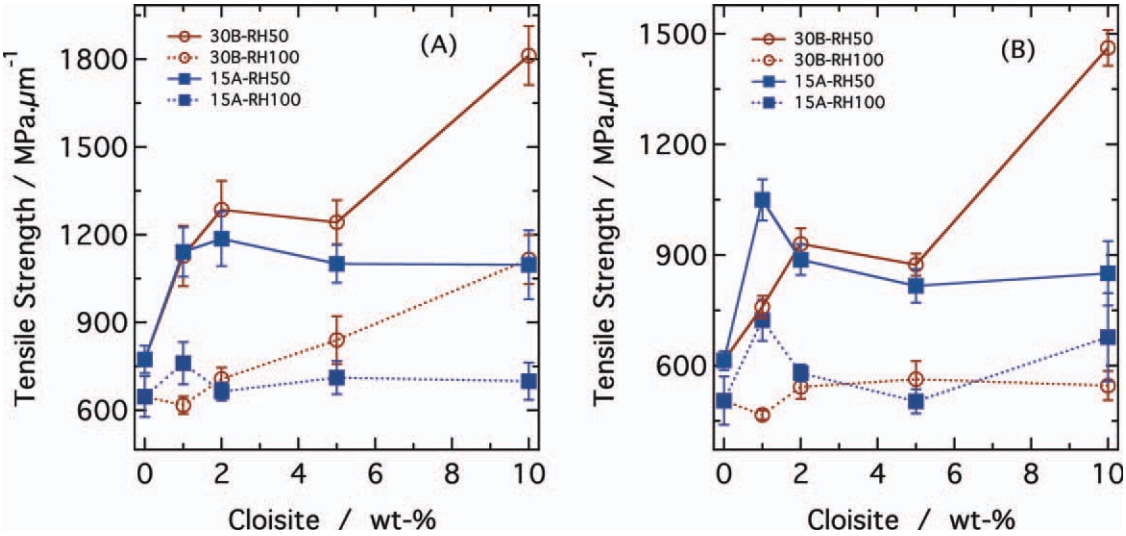

Figure 5 Comparison between the absolute traction force until rupture normalized by average thickness in the (A) machine and (B) transversal direction, for samples of pristine PA-6 and respective nanocomposites with 1, 2, 5, and 10 wt % Cloisite 15A and Cloisite 30B, conditioned at 50 and 100% relative humidity. [Color figure can be viewed in the online issue, which is available at wileyonlinelibrary.com.]

in Figure 4(C). In fact, the incorporation of higher amounts of organophillized MMT decrease the polymer chain mobility, but the aluminosilicate nanoflakes also can act as bridging sites.[43] Thus, there is a competition between these effects and the elongation is maximized in the nanocomposites with 1–2 wt % of Cloisite.

Furthermore, the mechanical properties of PA-6 are strongly influenced by humidity as it is hygroscopic and water act as a plasticizer. In fact, both parameters, tensile strength, and elongation, showed a significant decrease at 100% relative humidity as compared to 50%. It was proposed that water molecules interact with amide groups by strong and weak interactions, always breaking down the direct hydrogen bonds between amide groups connecting the PA-6 chains, thus decreasing the stiffness and elongation parameters.[44] Also, there are evidences that nanocomposites tend to absorb water more slowly than the pristine polymer matrix such that similar effects are observed after long enough exposition times.[45]

A comparison between the tensile strengths at 50 and 100% relative humidity (Fig. 5) confirmed the plasticizing effect of water discussed above. In fact, the enhancement gained in that property at 50% is almost completely lost at 100% relative humidity, where the measured parameters were only slightly better than the value for the pristine PA-6 in the same experimental conditions. The discrepancy of the data for the composite with 10 wt % Cloisite 30B probably is a consequence of the lower average thickness and much higher variability measured for that sample [Fig. 4(A)].

Another important property is the resistance to perforation, i.e., the resistance of the material to localized pressure. No significant change in this property (Force $\sim$ 22 N, average thickness $\sim$ 50 μm) was observed as a function of the amount of Cloisite, as shown in Supporting Information Figure S4. Nevertheless, there was a significant decrease in the elongation up to puncture, as a consequence of the stiffness enhancement caused by the incorporation of Cloisite, as discussed above.

Thermomechanical properties

Significant but minor effects were observed in the traction, puncture, and elongation until rupture, but the material can exhibit enhanced mechanical resistance at higher temperatures. Accordingly, the influence of the amount of Cloisite nanofiller and the degree of crystallinity on the flow characteristics of PA-6 composites in the MD was verified.

A striking effect was observed when the elongation of the samples until rupture at constant applied force was analyzed as a function of temperature, as shown in Figure 6. The pristine resin flowed quite easily even at 70°C stabilizing at about 200 μm, then elongating rapidly up to 3000 μm before rupture as the temperature rose until up to 120°C. All Cloisite 30B (Fig. 6) and Cloisite 15A nanocomposites exhibited similar thermomechanical behavior, but with a clear tendency of increasing stiffness as a function of the clay content. In fact, the slope is very low below 145°C, then increasing rapidly as a function of the temperature. However, even at the lowest clay content (1 wt %), it is possible to get almost the full

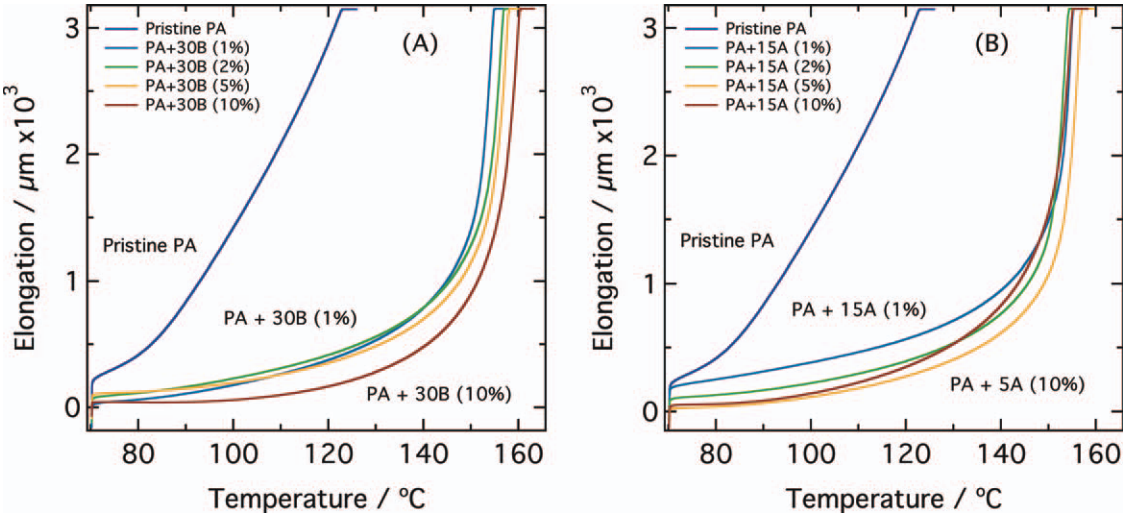

Figure 6 TMA data for samples of pristine PA-6 and PA-6 nanocomposite with (A) Cloisite 30B and (B) Cloisite 15A. [Color figure can be viewed in the online issue, which is available at wileyonlinelibrary.com.]

enhancement that can be obtained with 10 wt % of Cloisite, reflecting the major contribution of the γ-phase on the thermomechanical properties.

The exception to that behavior is the composite with 10 wt % of Cloisite 15A whose thermomechanical properties were worse than that of the composite with 5 wt % of that organoclay. This unexpected result may be assigned to the much more hydrophobic characteristics of the quaternary ammonium salt than that in Cloisite 30B, thus contributing to decrease the hydrogen bond interactions between the polymer chains. This is also reflecting on the higher tendency of the respective PCN films to flow at lower temperatures, as can be seen in Figure 6.

Gas permeation properties of the nanocomposite films

Experiments were carried out at 0 and 95% relative humidity to evaluate its influence on the permeability of those polymeric films to oxygen gas and water vapor. PA-6 exhibits a medium barrier for gas diffusion, i.e., the permeability for O_2 varies in the 20 and 60 $cm^3\ m^{-2}\ day^{-1}$, at 0% relative humidity. However, its polar nature is responsible for a relatively high permeability to vapor (400–1000 mg m^{-2} day^{-1} for 40–60-μm thick films). Clearly, the affinity of the perfusing gas or vapor for the polymer matrix strongly influences that property. On the other hand, the water molecules present in the structure also can

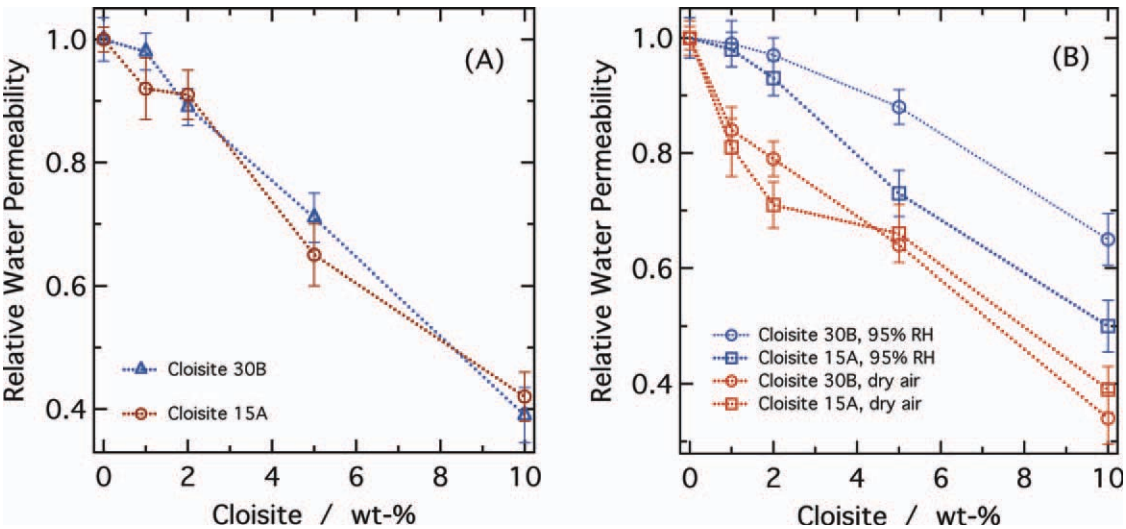

Figure 7 Relative permeability of (A) water vapor and (B) oxygen gas through PA-6/Cloisite nanocomposites as a function of the wt % of Cloisite nanofiller. [Color figure can be viewed in the online issue, which is available at wileyonlinelibrary.com.]

act as a plasticizer decreasing the intermolecular forces between the polymer chains.[46] As a consequence, small molecules can diffuse through more easily because there is more free space in the humidified polymeric material. However, the gas pathway will depend on the local mechanical properties, the degree of crystallinity and the temperature.

The PA-6/Cloisite nanocomposites have a much higher crystallinity than the pristine resin, thus should exhibit lower gas permeability. In addition, the presence of exfoliated MMT clay platelets dispersed in the material should contribute to increase the diffusion pathway, decreasing further the gas permeability[47] by the so-called tortuous path effect. Those effects are clearly reflected on the almost linear decrease of permeability to vapor as a function of wt % of Cloisite, as shown in Figure 7(A). It is interesting to note also that both organoclays gave similar results, leading to about 60% decrease relative to pristine PA-6 films at the highest concentration. A similar behavior was observed when the relative permeability of dry films to oxygen gas was evaluated. In both nanocomposites, there was up to about 20% decrease of permeability for 1 wt % of organoclay, followed by a less pronounced and monotonic linear decrease down to 38% for the composite with 10 wt % of Cloisite. Much significant differences were observed when the same test was carried out at 95% relative humidity. In this case, almost no barrier effect was observed for the composites with 1 wt % reflecting the plasticizing effect of water. However, the permeability decreased more or less linearly down to 65 (30B) and 50% (15A) at 10 wt %, as compared with the pristine PA-6 film [Fig. 7(B)). Accordingly, the hydrophilic/hydrophobic character of the quaternary ammonium salt used for the organophilization of MMT clay seems to plays a significant role by influencing the affinity and the plasticizing effect of water, and consequently the permeability of gases at higher relative humidity conditions.

CONCLUSIONS

A deconvolution method based on Gaussian curves was used to estimate the relative contributions of the amorphous and the crystalline γ- and α-phases on the structure of PA-6 nanocomposites as a function of the amount of Cloisite 15A and 30B nanofillers (1–10 wt % range). The presence of clay platelets strongly induced the organization of the polymer chains in the melt, favoring the formation of the γ-phase (up to ~ 50%) at expense of the amorphous phase, while the fraction of α-phase remained more or less constant (~ 10%). The tensile strength, resistance to puncture, elongation, and thermomechanical properties correlated well with the γ-phase fraction in the nanocomposites. The plasticizing effects of water at higher humidity conditions also played a significant role canceling out the enhancement accounted for by the crystallization of the polymer matrix. Thus, when only thermomechanical properties are considered, there is no significant advantage in using high concentrations of the organoclay nanofiller. However, higher concentrations of Cloisite should be used when barrier effects are being considered indicating that the tortuous path permeation mechanism is the predominant factor hindering the diffusion of gas or vapor molecules through the polymeric nanocomposite films.

The authors are grateful to the UNIPAC for the use of equipments and measurement of mechanical, thermomechanical, and gas diffusion properties of polymeric nanocomposites.

References

1. Sanchez, C.; Belleville, P.; Popall, M.; Nicole, L. Chem Soc Rev 2011, 40, 696.
2. Jancar, J.; Douglas, J. F.; Starr, F. W.; Kumar, S. K.; Cassagnau, P.; Lesser, A. J.; Sternstein, S. S.; Buehler, M. J. Polymer 2010, 51, 3321.
3. Robeson, L. M.; Paul, D. R. Polymer 2008, 49, 3187.
4. Usuki, A.; Hasegawa, N.; Kato, M. Adv Polym Sci 2005, 179, 135.
5. Hasegawa, N.; Okamoto, H.; Kato, M.; Usuki, A.; Sato, N. Polymer 2003, 44, 2933.
6. Sanchez, C.; Julian, B.; Belleville, P.; Popall, M. J Mater Chem 2005, 15, 3559.
7. Miltner, H. E.; Van Assche, G.; Pozsgay, A.; Pukanszky, B.; Van Mele, B. Polymer 2006, 47, 826.
8. Okada, A.; Usuki, A. Macromol Mater Eng 2006, 291, 1449.
9. Porter, D.; Metcalfe, E.; Thomas, M. J. K. Fire Mater 2000, 24, 45.
10. Wang, S.; Hu, Y.; Li, Z.; Wang, Z.; Zhuang, Y.; Chen, Z.; Fan, W. Colloid Polym Sci 2003, 281, 951.
11. Gilman, J. W. Appl Clay Sci 1999, 15, 31.
12. Morgan, A. B.; Harris, R. H. J.; Kashiwagi, T.; Chyall, L. J.; Gilman, J. W. Fire Mater 2002, 26, 247.
13. Vaia, R. A.; Ishii, H.; Giannelis, E. P. Chem Mater 1993, 5, 1694.
14. Awad, W. H.; Beyer, G.; Benderly, D.; Ijdo, W. L.; Songtipya, P.; Jimenez-Gasco, M. d. M.; Manias, E.; Wilkie, C. A. Polymer 2009, 50, 1857.
15. Dan, C. H.; Lee, M. H.; Kim, Y. D.; Min, B. H.; Kim, J. H. Polymer 2006, 47, 6718.
16. Bhattacharya, M.; Biswas, S.; Bhowmick, A. K. Polymer 2011, 52, 1562.
17. Cele, N.; Ray, S. S. Macromol Mater Eng 2009, 294, 719.
18. do Nascimento, G. M.; Constantino, V. R. L.; Landers, R.; Temperini, M. L. A. Polymer 2006, 47, 6131.
19. Ray, S. S.; Yamadab, K.; Okamoto, M.; Ueda, K. Polymer 2003, 44, 857.
20. Haraguchi, K.; Usami, Y.; Yamamura, K.; Matsumoto, S. Polymer 1998, 39, 6243.
21. Perotti, G. F.; Barud, H. S.; Messaddeq, Y.; Ribeiro, S. J. L.; Constantino, V. R. L. Polymer 2011, 52, 157.
22. Dennis, H. R.; Hunter, D. L.; Chang, D.; Kimb, S.; White, J. L.; Cho, J. W.; Paul, D. R. Polymer 2001, 42, 9513.
23. Fornes, T. D.; Paul, D. R. Polymer 2003, 44, 3945.

24. Liu, L.; Qi, Z.; Zhu, X. J Appl Polym Sci 1999, 71, 1133.
25. Russo, G. M.; Nicolais, V.; Maio, L. D.; Montesano, S.; Incarnato, L. Polym Degrad Stab 2007, 92, 1925.
26. Homminga, D. S.; Goderis, B.; Mathot, V. B. F.; Groeninckx, G. Polymer 2006, 47, 1630.
27. Wu, Q. J.; Liu, X. H.; Berglund, L. A. Macromol Rapid Commun 2001, 22, 1438.
28. Devaux, E.; Bourbigot, S.; El Achari, A. J Appl Polym Sci 2002, 86, 2416.
29. Katoh, Y.; Okamoto, M. Polymer 2009, 50, 4718.
30. Maiti, P.; Okamoto, M. Macromol Mater Eng 2003, 288, 440.
31. Miri, V.; Elkoun, S.; Peurton, F.; Vanmansart, C.; Lefebvre, J.-M.; Krawczak, P.; Seguela, R. Macromolecules 2008, 41, 9234.
32. Liu, X.; Wu, Q. Eur Polym J 2002, 38, 1383.
33. Lim, L.-T.; Britt, I. J.; Tung, M. A. J Appl Polym Sci 1999, 71, 197.
34. Zhao, X.-Y. Polym Int 2009, 58, 469.
35. Slusarczyk, C.; Binias, W.; Fabia, J.; Binias, D. Fibres Text East Eur 2007, 15, 22.
36. Lincoln, D. M.; Vaia, R. A.; Wang, Z.-G.; Hsiao, B. S.; Krishnamoorti, R. Polymer 2001, 42, 9975.
37. Morgan, A. B.; Gilman, J. W. J Appl Polym Sci 2003, 87, 1329.
38. Scocchi, G.; Posocco, P.; Fermeglia, M.; Pricl, S. J Phys Chem B 2007, 111, 2143.
39. Yebra-Rodriguez, A.; Alvarez-Lloret, P.; Rodriguez-Navarro, A. B.; Martin-Ramos, J. D.; Cardell, C. Mater Lett 2009, 63, 1159.
40. Fornes, T. D.; Hunter, D. L.; Paul, D. R. Macromolecules 2004, 37, 1793.
41. Wilkinson, A. N.; Man, Z.; Stanford, J. L.; Matikainen, P.; Clemens, M. L.; Lees, G. C.; Liauw, C. M. Compos Sci Technol 2007, 67, 3360.
42. Shelley, J. S.; Mather, P. T.; DeVries, K. L. Polymer 2001, 42, 5849.
43. Tamura, K.; Uno, H.; Yamada, H.; Umeyama, K. J Polym Sci B: Polym Phys 2009, 47, 583.
44. Picard, E.; Gérard, J. F.; Espuche, E. J Membr Sci 2008, 313, 284.
45. Vlasveld, D. P. N.; Groenewold, J.; Bersee, H. E. N.; Picken, S. J. Polymer 2005, 46, 12567.
46. Hu, Y. S.; Mehta, S.; Schiraldi, D. A.; Hiltner, A.; Baer, E. J Polym Sci 2005, 43, 1365.
47. Tyan, H.-L.; Wu, C.-Y.; Wei, K.-H. J Appl Polym Sci 2001, 81, 1742.